Purdue University
Purdue e-Pubs

Civil Engineering Faculty Publications   Civil Engineering

7-2-2010

Effect of Relative Density and Stress Level on the Bearing Capacity of Footings on Sand

Rodrigo Salgado
Purdue University, rodrigo@ecn.purdue.edu

Follow this and additional works at: http://docs.lib.purdue.edu/civeng

Part of the Civil and Environmental Engineering Commons

Effect of relative density and stress level on the bearing capacity of footings on sand

D. LOUKIDIS* and R. SALGADO†

The design of shallow foundations relies on bearing capacity values calculated using empirical procedures that are based in part on solutions obtained using the method of characteristics, which assumes a soil that is perfectly plastic following an associated flow rule. In this paper the problem of strip and circular footings resting on the surface of a sand layer is analysed using the finite-element method. Analyses are performed using a two-surface plasticity constitutive model that realistically captures the aspects of the mechanical response of sands that are relevant to the bearing capacity problem. In particular, the model accounts for non-associated flow, strain-softening, and both stress-induced and inherent anisotropy. Based on the results of the analyses, the paper examines the validity of the bearing capacity factors N_γ and shape factors s_γ used in practice. A relationship for determining appropriate values of friction angle for use in bearing capacity calculations is also proposed.

KEYWORDS: anisotropy; bearing capacity; footings/foundations; numerical modelling; plasticity; sands

L'étude de fondations peu profondes repose sur des valeurs de force portante calculées en utilisant des procédures empiriques, basées en partie sur des solutions obtenues avec la méthode des caractéristiques, qui présuppose la présence d'un sol parfaitement plastique en suivant une règle d'écoulement connexe. Dans la présente communication, on a analysé le problème de semelles filantes et circulaires posées sur la surface d'une couche de sable, avec la méthode aux éléments finis. Des analyses ont été effectuées en utilisant un modèle constitutif de plasticité de deux surfaces, exprimant, de façon réaliste, les aspects de la réaction mécanique des sables dans le contexte du problème de la force portante. Ce modèle se penche notamment sur le débit non associé, sur le radoucissement, ainsi que sur l'anisotropie par pression et inhérente. Sur la base des résultats des analyses, la communication examine la validité des facteurs de force portante N_γ et des facteurs de forme s_γ utilisés dans la pratique. En outre, on propose également un rapport pour la détermination de valeurs appropriées de l'angle de frottement pour les calculs de la force portante.

INTRODUCTION

For a vertically loaded footing resting on the surface of an uncemented sand deposit (in which case both surcharge q_0 and soil cohesion c are zero), the bearing capacity equation reduces to

$$q_{bL} = \tfrac{1}{2}\gamma' B N_\gamma s_\gamma \qquad (1)$$

where γ' is the soil effective unit weight, B is the footing width, N_γ is the bearing capacity factor and s_γ is the shape factor that introduces the effect of footing geometry for footings other than strip footings. The most popular expressions for N_γ – by Meyerhof (1963), Brinch Hansen (1970) and Vesić (1973) – are based on solutions obtained using the method of characteristics (MOC). The most recent analysis of this type is that of Martin (2005), which produces N_γ values that are shown to be nearly exact. Rigorous lower and upper bounds by Lyamin *et al.* (2007) provide extra corroboration for the validity of the Martin (2005) solution, which can be closely approximated by the expression

$$N_\gamma = (N_q - 0.6)\tan(1.33\phi') \qquad (2)$$

where

$$N_q = \left(\frac{1 + \sin\phi'}{1 - \sin\phi'}\right)\exp\left(\pi\tan\phi'\right)$$

and ϕ' is the effective friction angle of the soil.

The method of characteristics and limit analysis assume that the soil is perfectly plastic and follows an associated flow rule (dilatancy angle ψ_{dil} equal to ϕ'), although it is well known that, for sands, ψ_{dil} is significantly lower than ϕ'. In addition, the peak value of the effective friction angle ϕ' depends strongly on the relative density D_R and on the level of mean effective stress p'. The angle ϕ' decreases with decreasing D_R and increasing p'. Both D_R and p' evolve continuously in the vicinity of the footing during the loading process. So there are parts of the collapse mechanism (Fig. 1) where the peak ϕ' is high (in the low-stress regions of the passive wedges) and parts where the peak ϕ' is low (in the high-stress region, close to the footing base).

Certain regions below the footing will fail and start to soften early in the loading process. The shear strain level developed in these regions may be large enough for ϕ' to drop to its critical-state value ϕ_c before the footing's limit load is reached. The effect of progressive failure is more prominent in the case of footings with small B, since the brittleness of sands increases with decreasing p' (Perkins & Madson, 2000). Additionally, the ϕ' value for strip footings (plane-strain conditions) is higher than that for square or circular footings, for which the mode of deformation is closer to triaxial conditions. This difference is due to the effect of the different intermediate principal stress ratios b ($= (\sigma_2' - \sigma_3')/(\sigma_1' - \sigma_3')$). Meyerhof (1963) suggested the use of values of peak friction angle that are higher (by 10%) for strip footings than for square or circular footings.

Finally, the mechanical behaviour of most sands in the field is anisotropic. The inherent (fabric-related) anisotropy originates mainly from the fact that, during the deposition of the sand, its particles tend to settle with their longest axis predominantly parallel to the horizontal plane (Oda, 1972). Experimental studies have shown that, as the angle between the direction of the increment of the major principal effec-
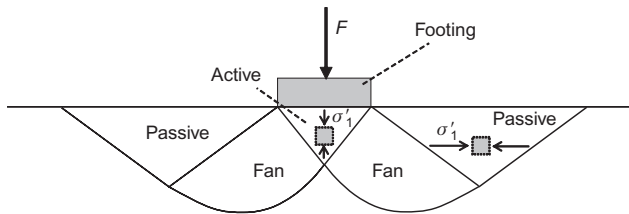
Fig. 1. Schematic of bearing capacity collapse mechanism as predicted by classical plasticity

tive stress σ'_1 and the direction of sand deposition increases, the sand response becomes increasingly less dilative (e.g. Nakata *et al.*, 1998; Yoshimine *et al.*, 1998) and ϕ' becomes smaller (e.g. Tatsuoka *et al.*, 1986; Lam & Tatsuoka, 1988; Abelev & Lade, 2004). Given that the direction of σ'_1 varies significantly inside the collapse mechanism, the inherent anisotropy of the sand should have a significant impact on the bearing capacity of a footing.

All of these factors (mean effective stress, intermediate principal stress, relative density, progressive failure, inherent anisotropy, and non-associativity) render the appropriate N_γ value an unknown that is very difficult to determine. This study attempts to address this issue through finite-element (FE) simulations of the bearing capacity problem of strip and circular footings resting on the free surface (and thus with zero embedment) of frictional soils. The FE analyses employ a two-surface plasticity model that takes into account both inherent and stress-induced anisotropy, and reproduces correctly the dependence of the sand strength and dilatancy on mean effective stress level, strain level and relative density.

FINITE-ELEMENT SIMULATIONS
Constitutive model

The constitutive model used in this study is the two-surface plasticity model originally developed by Manzari & Dafalias (1997) and subsequently improved and expanded by Li & Dafalias (2000), Papadimitriou & Bouckovalas (2002) and Dafalias *et al.* (2004). Certain additional modifications (the equations marked with an asterisk in Table 1) were made to this model in order to improve the simulation of experimental data, and capture aspects of sand behaviour that are important in the analysis of foundations (Loukidis, 2006; Loukidis & Salgado, 2009a). The model parameters were determined for two sands: air-pluviated/dry-deposited Toyoura sand (Iwasaki *et al.*, 1978; Fukushima & Tatsuoka, 1984; Lam & Tatsuoka, 1988; Yoshimine *et al.*, 1998) and water-pluviated/slurry-deposited clean Ottawa sand (Carraro *et al.*, 2003; Carraro, 2004; Murthy, 2006; Murthy *et al.*, 2007). Toyoura sand has mean particle size $D_{50} \approx 0.19$ mm, and Ottawa sand has mean particle size $D_{50} \approx 0.39$ mm. Although both are silica sands, and have fairly uniform grain size distributions, they differ significantly in particle size and angularity, with Toyoura sand particles being angular to sub-angular and Ottawa sand particles being rounded to sub-rounded. The model is compatible with the framework of critical-state soil mechanics, taking the inherent anisotropy of sands into account through the use of a fabric tensor (Dafalias *et al.*, 2004). Details of the constitutive model formulation, the determination of its input parameters, and its use in simulating element response in laboratory tests can be found in Loukidis (2006) and Loukidis & Salgado (2009a). The constitutive model formulation is summarised in Table 1. A summary of the model can also be found in Loukidis & Salgado (2008). The model parameters for air-pluviated/dry-deposited Toyoura sand and water-pluviated/slurry-deposited Ottawa sand are given in Table 2.

Finite-element formulation

The FE analyses were performed using the code SNAC (Abbo & Sloan, 2000), in which the two-surface constitutive model was implemented. The analyses use unstructured meshes consisting of 15-noded (cubic-strain) triangular elements (Fig. 2). The stress–strain rate equations of the constitutive model were integrated using a semi-implicit Euler algorithm with sub-incrementation and error control, details of which can be found in Loukidis (2006). The plane-strain elements used in the strip footing simulations and the axisymmetric elements used in the circular footing simulation possessed 12 and 16 Gauss-quadrature points respectively, following Sloan & Randolph (1982).

Loading is applied on the footing by prescribing uniform incremental vertical displacements and zero horizontal displacements at the nodes defining the footing/soil interface (characterising a perfectly rigid footing). There are no interface elements at the soil/footing interface, so any slippage between footing and soil occurs within the soil. This is realistic, because concrete footings poured against the ground form a very rough interface. Typical mesh and boundary conditions are shown in Fig. 2. The distances of the bottom and lateral boundaries from the footing varied from analysis to analysis in order to ensure that the boundaries did not interfere with the development of the collapse mechanism, and that their influence on the collapse load value was insignificant.

The FE analyses were performed using the modified Newton–Raphson global solution scheme with the elastic stiffness matrix as the global stiffness matrix. All analyses start with an initial stage in which the geostatic stress field is established in the FE mesh. During this initial stage the desired initial (geostatic) stresses are prescribed at every Gauss-quadrature point in the mesh. The kinematic hardening stress (normalised deviatoric back-stress) tensor (equation (23) in Table 1) is initialised such that the stresses lie on the axis of the conical yield (loading) surface (equation (10) in Table 1) (i.e. the stress state is at the centre of the elastic domain in the deviatoric plane). Then a single global solution step is performed, in which the gravity (body) forces are applied in one increment (i.e. instantaneously). Because the initial vertical stress values are set to be consistent with applied gravity loading, equilibrium is reached instantly. The footing loading stage that follows consists of a large number (of the order of 10^5) of constant-size increments with a number of 10–20 equilibrium-correction iterations. Using this configuration, the ratio of the maximum unbalanced force to the maximum external nodal force (a ratio usually referred to as the unbalanced force norm) did not exceed 0.001.
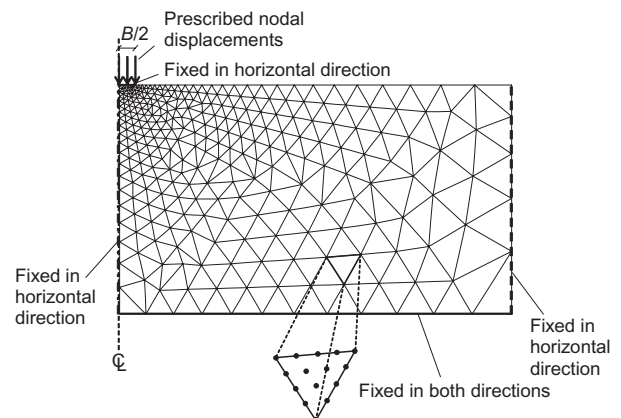

Fig. 2. Typical mesh and boundary conditions for footing simulations

RESULTS OF FINITE-ELEMENT SIMULATIONS

Analyses were performed for values of footing width B ranging from 1 m to 3 m, and sand effective unit weight γ' ranging from 10 kN/m^3 (effective unit weight for water table at the ground surface, i.e. buoyant unit weight) to 20 kN/m^3 (effective unit weight of wet sand above the water table with the water table at depth below the footing). As will be demonstrated in subsequent sections, the choice of the sand unit weight is immaterial, since the results can be normalised almost perfectly with respect to the product $\gamma'B$. In most of the analyses, the coefficient K_0 was set equal to 0·5. A few runs were performed using $K_0 = 0·4$ for comparison.

General response in strip footing analyses

Figure 3 shows the load–settlement response from analyses of strip footings with $B = 2$ m. As expected, the bearing capacity increases with increasing D_R. Apart from the global maximum, which corresponds to the collapse (limit) load Q_L in the classical sense, the load–displacement
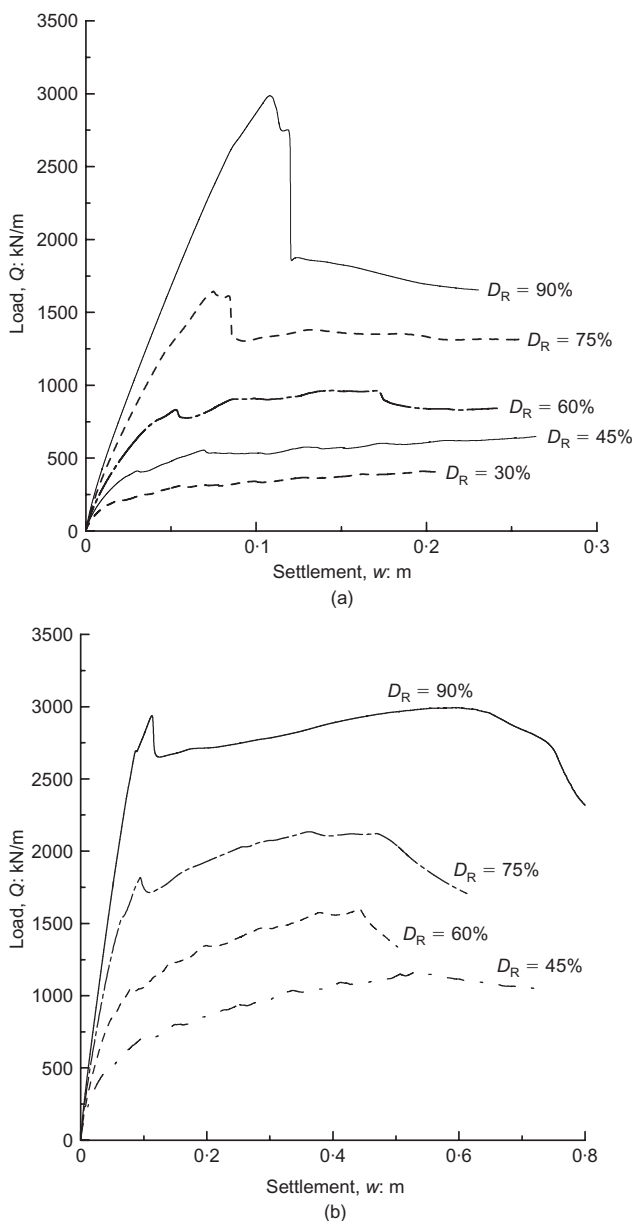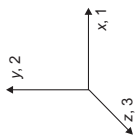

Fig. 3. Load–settlement response from analyses of 2 m wide strip footing: (a) on Toyoura sand with effective unit weight 10 kN/m^3; (b) on clean Ottawa sand with effective unit weight equal to 20 kN/m^3

curves demonstrate local maxima and minima due to numerical oscillations. These oscillations are a direct consequence of the strain-softening and flow rule non-associativity, which result in energy being released during intense shear banding. The energy that is released locally is transferred/absorbed in the regions where localisation has not started yet. The oscillations observed in the response of full-scale footing loading tests in the field or physical model tests in the laboratory are again a result of localisation and energy release in the actual granular material. Of course, neither the intensity nor the frequency of the pattern of oscillations observed in numerical analyses is expected to match that observed in reality, since the numerical simulations using a constitutive model that is based on the macroscopic sand response observed in laboratory tests, a Cauchy continuum and finite elements do not constitute exact representations of the true physical process at the micromechanical level.

In simulations of strip footings on clean Ottawa sand (Fig. 3(b)), the load–displacement response is less brittle than on Toyoura sand (Fig. 3(a)). This may be attributed to the fact that Ottawa sand has rounded to sub-rounded particles, whereas Toyoura sand particles are angular to sub-angular, a difference that renders Ottawa sand less brittle and less strong than Toyoura sand. Nonetheless, a minor local peak occurs at a settlement value w that is approximately 5% of the footing width B for dense sand ($D_R \geqslant 75\%$).

Generally, the FE results of this study show that the limit load in dense sand is reached at settlements w_L in the range 0·04B to 0·30B. Vesić (1973) reports w_L values for surface footings resting on cohesionless soil in the range 0·05B to 0·15B. Centrifuge tests on dense F75 silica sand ($D_R = 88\%$) by Aiban & Znidarčić (1995) yield settlements at the limit load of about 0·1B. Model tests at 1g and centrifuge tests of strip footings by Tatsuoka *et al.* (1991) exhibit w_L of the order of 0·05–0·07B and 0·10–0·20B respectively. Centrifuge tests on Toyoura sand ($D_R = 60–90\%$) by Kimura *et al.* (1985) reach the limit load at settlements in the range 0·06B to 0·2B, with the larger values corresponding to the smaller relative densities.

One might expect that reaching Q_L would always coincide with the formation of the general shear collapse mechanism (Vesić, 1973), where the slip surface originating from the tip of the active wedge propagates and reaches the free surface (Fig. 1). However, the present analyses suggest that full formation of a general shear collapse mechanism (GSCM) requires large settlements, and is not strictly associated with the attainment of Q_L. Figs 4(b) and 5(a) show contours of incremental plastic maximum shear strain $\Delta\gamma^p_{max}$ from an analysis of strip footings on Toyoura sand and clean Ottawa sand respectively, with $D_R = 75\%$. Although w is clearly larger than w_L, the GSCM is not yet fully formed, with shear bands that define the active (rigid) wedge below the footing and only a part of the shear band forming the bottom boundary of the fan zone developed; elsewhere in the footing vicinity there is plastic shearing, but this is in the form of diffused deformation that is not localised in shear bands. This incomplete mechanism allows the footing to move downwards easily while pushing aside the soils in the region adjacent to the active wedge. The complete GSCM will eventually form with further increase of w (Fig. 5(b)). The fact that the attainment of Q_L may precede the formation of the GSCM has been observed in 1g model tests by Tatsuoka *et al.* (1991) and in centrifuge tests by Aiban & Znidarčić (1995). In addition, FE element analyses show that a fully developed GSCM also forms in sand with D_R as low as 45% (Fig. 6) provided the footing is pushed to large settlements (0·25–0·5B), in which case the w_L is more likely to correspond to full formation of GSCM.

At settlements of the order of 0·2–0·3B the footing has

Table 1. Equations of two-surface plasticity constitutive model

Description	Equation number	Constitutive equations	Parameters	References/notes
Stress–strain relations	(6)	$\dot{\sigma}'_{ij} = 2G(\dot{\varepsilon}_{ij} - \dot{\varepsilon}^p_{ij}) + \left(K - \frac{2}{3}G\right)(\dot{\varepsilon}_{kk} - \dot{\varepsilon}^p_{kk})\delta_{ij}$	–	–
Small-strain shear modulus	(7)*	$G_{max} = C_g \dfrac{(2\cdot17 - e)^2}{1+e} p'^{n_g} p_A^{1-n_g}$	C_g, n_g	Hardin & Richart (1963)
Elastic shear modulus with Ramberg–Osgood degradation	(8)	$G = \dfrac{G_{max}}{1 + 2\left(\dfrac{1}{\alpha_1} - 1\right)\left[\dfrac{\sqrt{\frac{3}{2}}\sqrt{(r_{ij} - a_{ij,ini})(r_{ij} - a_{ij,ini})}}{2\alpha_1(G_{max}/p')\gamma_1}\right]} \geq \dfrac{G_{max}}{1 + 2\left(\dfrac{1}{\alpha_1} - 1\right)}$	α_1, γ_1	Papadimitriou & Bouckovalas (2002)
Elastic bulk modulus	(9)	$K = \dfrac{2(1+\nu)}{3(1-2\nu)}G$	ν	–
Yield (loading) surface	(10)	$f = \sqrt{(s_{ij} - a_{ij}p')(s_{ij} - a_{ij}p')} - \sqrt{\frac{2}{3}}mp' = 0$	m	Manzari & Dafalias (1997)
Plastic multiplier	(11)	$\dot{\Lambda} = \dfrac{1}{H}\left[n_{ij} - \dfrac{1}{3}(n_{kl}r_{kl})\delta_{ij}\right]\dot{\sigma}'_{ij}$ where $n_{ij} = (r_{ij} - a_{ij})/\sqrt{(r_{ij} - a_{ij})(r_{ij} - a_{ij})}$ and $r_{ij} = s_{ij}/p'$	–	Manzari & Dafalias (1997)
Bounding, dilatancy and CS surfaces	(12a), (12b), (12c)	$M_b = g(\theta)M_{cc}\exp(-k_b\psi), \; M_d = g(\theta)M_{cc}\exp(k_d\psi), \; M_c = g(\theta)M_{cc}$	M_{cc}, k_b, k_d	Li & Dafalias (2000)
State parameter and CSL in e–p'	(13a), (13b)	$\psi = e - e_c, \; e_c = \Gamma - \lambda(p'/p_A)^\xi$	λ, ξ	Li et al. (1999)
Shape of bounding, dilatancy and CS surfaces in the π plane	(14)*	$g(\theta) = 2^{n_s}c_1/[1 + c_1^{1/n_s} - (1 - c_1^{1/n_s})\cos(3\theta)]^{n_s}$	c_1, n_s	Modified expression
Plastic modulus	(15a)*, (15b)*	$H = h_0 h_k \sqrt{\dfrac{2}{3}} \dfrac{G\exp(k_b\psi)\left[\sqrt{\frac{2}{3}}(M_b - m) - a_{ij}n_{ij}\right]}{\left[\sqrt{\frac{3}{2}}\sqrt{(r_{ij} - a_{ij,ini})(r_{ij} - a_{ij,ini})}\right]^\mu}, \; h_0 = \left(\dfrac{e_{lim} - e}{h_2}\right)^{h_1}$	$h_1, h_2,$ e_{lim}, μ	Modified expression for h_0; Addition of exponent μ
Flow rule	(16a), (16b)	$\dot{\varepsilon}^p_{ij} = \dot{\Lambda}\left(R'_{ij} + \dfrac{1}{3}D\delta_{ij}\right), \; R'_{ij} = R'^*_{ij}/\sqrt{R'^*_{ij}R'^*_{ij}}$		Dafalias & Manzari (2004)
	(16c)	$R'^*_{ij} = \left[1 + \dfrac{3}{2}\left(\dfrac{1-c_2}{c_2}\right)g_2(\theta)\cos(3\theta)\right]n_{ij} - \left[3\sqrt{\dfrac{3}{2}}\left(\dfrac{1-c_2}{c_2}\right)g_2(\theta)\right]\left(n_{ik}n_{kj} - \dfrac{1}{3}\delta_{ij}\right)$	c_2	Normalisation of R'_{ij}
Dilatancy	(17)	$D = \dfrac{D_0}{M_{cc}}\left[\sqrt{\dfrac{2}{3}}(M_d - m) - a_{ij}n_{ij}\right]$	D_0	Manzari & Dafalias (1997)
Shape of plastic potential in π plane	(18)*	$g_2(\theta) = 2c_2/[(1 + c_2) - (1 - c_2)\cos(3\theta)]$	c_2	$c_2 \neq c_1$

Description	Eq.	Equation	Parameter	Reference
Fabric tensor	(19)	$F_{11} = F_{33} = 0.5(1 - \alpha)$, $F_{22} = \alpha$; $F_{ij} = 0$ for $i \neq j$	α	Dafalias et al. (2004)
Fabric-dependent scalar	(20)	$A_f = g(\theta)(F_{ij}n_{ij})$	–	Dafalias et al. (2004)
Fabric effect multiplier in H	(21a)*, (21b)*	$h_k = \exp\{[(A_{fc} - A_f)/(A_{fc} - A_{fe})]^{1\cdot25}\ln(k_h)\}$, $A_{fc} = -(1/c_1)A_{fe} = \sqrt{\frac{3}{2}}\left(\alpha - \frac{1}{3}\right)$	k_h	Modified h_k expression
Intercept of CSL	(22)*	$\Gamma = \Gamma_c \exp(A_{fc} - A_f)$	Γ_c	CSL in TXC is independent of fabric
Kinematic hardening of yield surface	(23)	$\dot{a}_{ij} = \dot{\Lambda}\dfrac{H}{p'}\left[\sqrt{\dfrac{2}{3}}(M_b - m)n_{ij} - a_{ij}\right]\bigg/\left[\sqrt{\dfrac{2}{3}}(M_b - m) - a_{ij}n_{ij}\right]$	–	Manzari & Dafalias (1997)

G = current value of shear modulus; K = bulk modulus; H = plastic modulus; σ'_{ij} = effective stress tensor; s_{ij} = deviatoric stress tensor; p' = mean effective stress; a_{ij} = kinematic hardening tensor; $a_{ij,\text{ini}}$ = initial value of kinematic hardening tensor; δ_{ij} = Kronecker's delta; ε_{ij} = strain tensor; Λ = plastic multiplier; ε^p_{ij} = plastic strain tensor.
*Equations revised by the authors.

Table 2. Constitutive model input parameters

	Parameter symbol	Parameter value		Test data required
		Toyoura sand (dry-deposited/ air-pluviated)	Clean Ottawa sand (slurry-deposited/ water-pluviated)	
Small-strain ('elastic') parameters	ν	0·15	0·15*	Tests using local strain transducers or isotropic compression or 1D compression tests with unloading path
	C_g	900	611	Bender element or resonant column tests
	n_g	0·400	0·437	Bender element or resonant column tests
	γ_1	0·0010	0·00065	Resonant column tests or triaxial tests with local strain measurements
	α_1	0·40	0·47	Undrained triaxial compression tests
Critical state parameters	Γ_c	0·934	0·780	Triaxial compression tests
	λ	0·019	0·081	Triaxial compression tests
	ξ	0·70	0·196	Triaxial compression tests
	M_{cc}	1·27	1·21	Triaxial compression tests
Bounding surface	k_b	1·5	1·9	Triaxial compression tests
Dilatancy	D_o	0·90	1·31	Triaxial compression tests
	k_d	2·8	2·2	Triaxial compression tests
Plastic modulus	h_1	1·62	2·20	Triaxial compression tests
	h_2	0·254	0·240	Triaxial compression tests
	e_{lim}	1·00	0·81	Triaxial compression tests
	μ	2·0	1·2	Undrained triaxial compression tests
Stress-induced anisotropy	c_1	0·72	0·71	Triaxial extension tests
	c_2	0·78	0·78*	Simple shear or other plane-strain tests
	n_s	0·35	0·35*	Simple shear or other plane-strain tests
Inherent anisotropy	α	0·29	0·31	Triaxial extension tests
	k_h	0·11	0·39	Triaxial extension tests
Yield surface radius	m	0·05	0·05	

* Assumed.

embedded itself into the soil by a non-negligible amount. The present FE analyses do not account for the increase in embedment during loading, as they employ a small-strain formulation. Because of the increase of embedment as the footing penetrates into the soil, the actual Q_L values should be greater than those produced by the FE analyses using a small-strain formulation.

The effect of the coefficient of earth pressure at rest on the bearing capacity is illustrated in Fig. 7. The bearing capacity increases with increasing K_0. This is because of the higher level of lateral confinement in the analyses with $K_0 = 0.5$ than in those with $K_0 = 0.4$, which, despite the slightly lower dilatancy for $K_0 = 0.5$ (because of the larger p'), leads to an overall increase of the collapse load. According to the FE results, an increase in the level of initial mean effective stress by 11%, due to an increase in K_0, leads to an increase of the limit load by 6–19%.

It is well known that analyses involving materials that soften and follow a non-associated flow rule suffer from the problem of solution non-uniqueness. This means that, as the mesh gets refined, the FE analysis results keep changing, without converging to a unique solution. If progressive failure were not a factor in the problem studied herein (i.e. if the peak stress state were reached simultaneously at all points in the failure mechanism), the FE analysis would produce a unique solution in terms of peak (collapse) load, since bifurcation and strain localisation would not precede the attainment of the collapse load. However, progressive failure is present in the problem studied herein, as certain points in the failure mechanism pass the peak stress state and proceed towards critical state before the footing collapse load is reached. In this case it is expected that there will be a certain degree of mesh dependence in relation to the strain localisation and bifurcation that occur before reaching the

collapse load. To examine the effect of element size, additional analyses were performed for the case of a strip footing with $B = 2$ m, $\gamma' = 20$ kN/m³ and Ottawa sand with $D_R = 90\%$ with meshes that have roughly 0·5 (2261 nodes) and 2 (8863 nodes) times the number of nodes of the mesh used in the main series of analyses (4397 nodes). The way the domain is meshed and the relative distribution of the elements are the same in all analyses. The results from the analyses with the three different mesh refinements are shown in Fig. 8. This figure shows that the effect of the density of the elements in the mesh (i.e. the element size) decreases with mesh refinement. The difference in collapse load between the main series analysis and that with twice as many nodes is 5%, whereas the difference between the main series analysis and that with half as many nodes is 14%.

General response in circular footing analyses

Figure 9 shows the load–settlement response for circular footings on Toyoura sand. The response is much smoother than that exhibited by the strip footing analyses. This can be explained by the fact that in the circular footing problem failure planes can form in virtually any direction, whereas in the strip footing analyses the kinematic constraint of plane-strain (PS) conditions forces the strike of the failure planes to be parallel to the strip footing axis. The absence of such constraint in the axisymmetric problem leads to a more diffused deformation pattern and a plastic strain localisation that is much less intense than in strip footings. This qualitative difference with respect to the smoothness and ductility of the load–settlement curves of circular and strip footings is analogous to that observed between the stress–strain curves of triaxial compression and plane-strain compression tests. Fig. 10 shows the $\Delta\gamma_{max}^p$ in an analysis of a circular
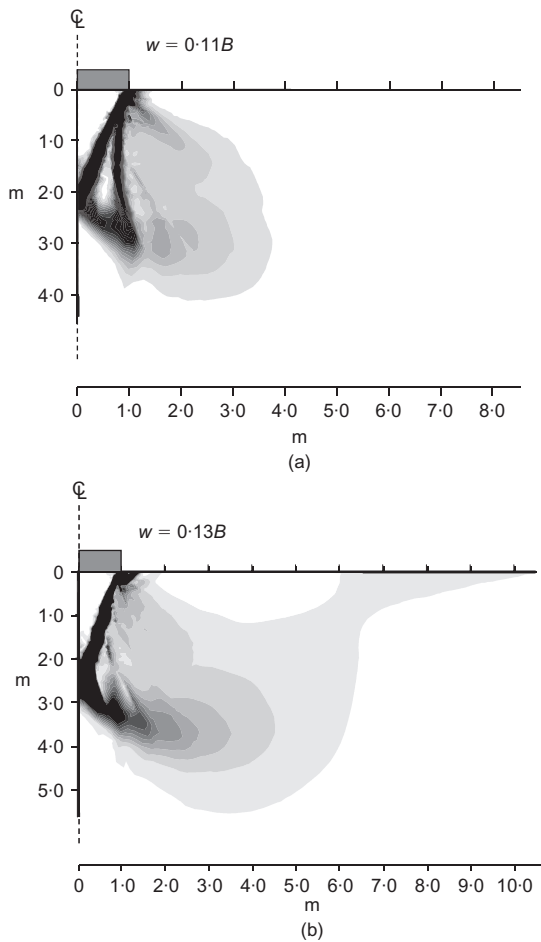
Fig. 4. Contours of incremental plastic maximum shear strain from analyses of 2 m wide strip footing on: (a) loose Toyoura sand ($\gamma' = 20$ kN/m³, $D_R = 45\%$); (b) dense Toyoura sand ($\gamma' = 10$ kN/m³, $D_R = 75\%$)

footing on dense Toyoura sand for w well beyond w_L. It can be seen that the active region develops under the footing in the form of a cone. However, the active cone does not appear to be rigid, since a rather significant amount of plastic shearing occurs inside it. Most importantly, a shear band encompassing a fan zone does not develop. Instead, there is intense plastic shearing adjacent to the active cone, which then dissipates in the radial direction. It can be argued that this mechanism resembles the deformation pattern of a cylindrical or spherical cavity expansion, as suggested by Vesić (1973).

According to the FE analyses of circular footings, the settlement required to reach Q_L, with only a few exceptions, is inside the range $0.035–0.067B$. Centrifuge tests of circular footings on dense Monterey 0/30 sand ($D_R \approx 94\%$) by Kutter *et al.* (1988) show w_L in the range $0.03–0.09B$ range. Based on data compiled by De Beer (1965), w_L is in the range $0.05–0.09B$ range.

Effect of pressure level on bearing capacity

Researchers have pointed out for decades that the bearing capacity factor N_γ decreases as the footing size increases. This observation has been often referred to as the size (or scale) effect. A number of studies investigating the scale effect – both experimental (e.g. Kimura *et al.*, 1985; Kutter *et al.*, 1988; Tatsuoka *et al.*, 1991, 1997; Ueno *et al.*, 1998) and numerical/analytical (e.g. Siddiquee *et al.*, 1999; Tejchman & Herle, 1999; Perkins & Madson, 2000; Ueno *et al.*, 2001) – have been published in the literature. There are
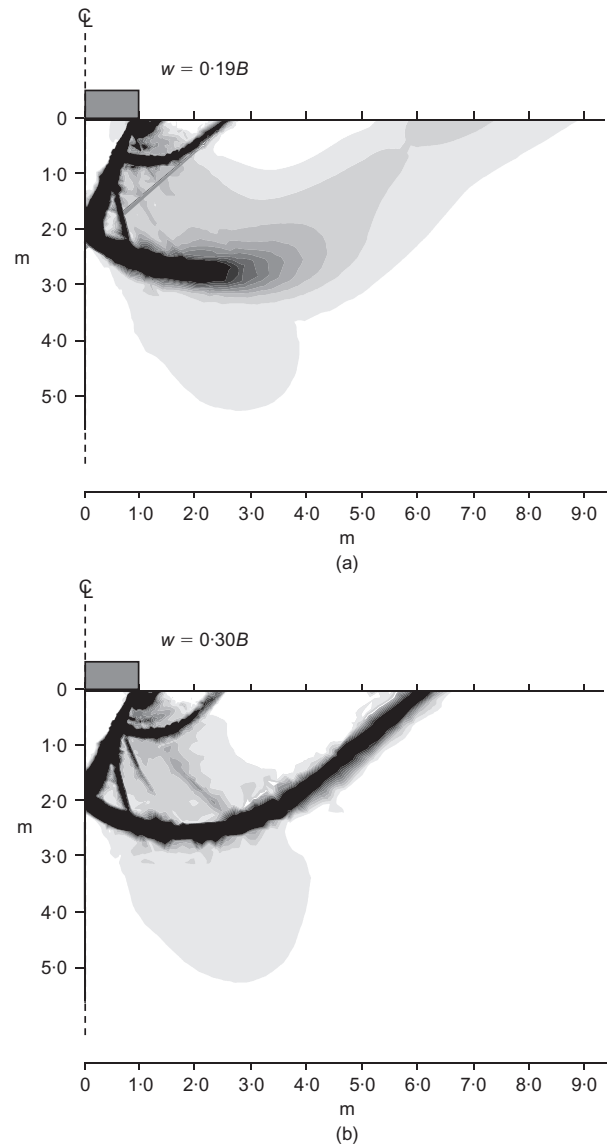

Fig. 5. Contours of incremental plastic maximum shear strain showing the evolution of the collapse mechanism for a 2 m wide strip footing on dense clean Ottawa sand ($\gamma' = 20$ kN/m³, $D_R = 75\%$)

two distinct factors that contribute to the scale effect. The first is the dependence of the sand peak friction angle on p'. A large B leads to increased q_{bL} and, consequently, increased average p' and reduced average ϕ' in the collapse mechanism. The second factor is mostly relevant to the small-scale testing frequently employed by researchers to study bearing capacity. As demonstrated by Tatsuoka *et al.* (1991, 1997) and Tejchman & Herle (1999), N_γ becomes larger at an increasing rate as the ratio D_{50}/B becomes larger. This is usually called the particle size effect. Unlike the pressure level effect, the particle size effect is not an issue in footings encountered in practice, since the footing widths used in construction are at least three orders of magnitude larger than D_{50}. Therefore it is appropriate to clearly distinguish the pressure-level effect from the particle-size effect.

The pressure level effect is clearly demonstrated in Fig. 11, which shows the normalised footing load (mobilised N_γ) plotted against normalised settlement w/B for footings resting on sand with the same characteristics but different footing widths. The figure shows that the peak normalised footing load decreases with increasing B. An interesting observation is that the response of the footing with $B = 2$ m but on a sand with $\gamma' = 10$ kN/m³ is almost identical to the
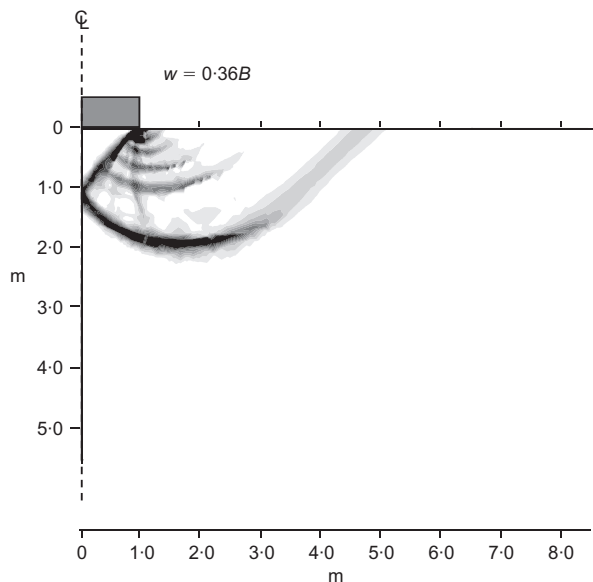
Fig. 6. Contours of incremental plastic maximum shear strain showing the collapse mechanism at large settlement for a 2 m wide strip footing on loose clean Ottawa sand ($\gamma' = 20$ kN/m^3, $D_R = 45\%$)
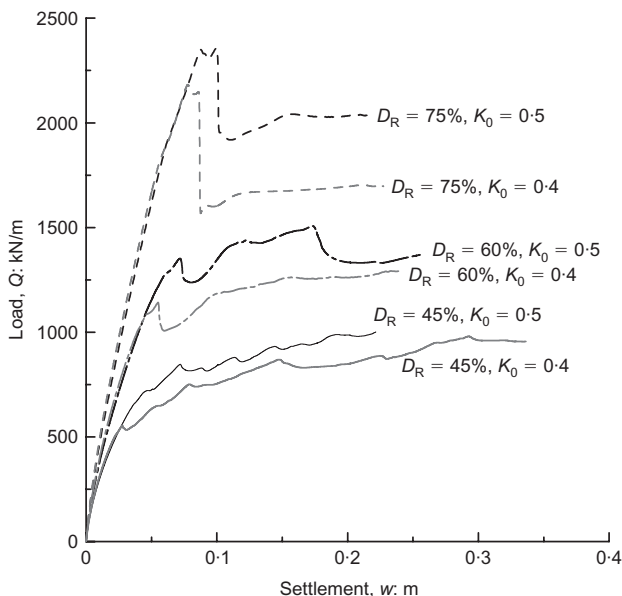

Fig. 8. Load–settlement response of 2 m wide strip footing on clean Ottawa sand with $D_R = 90\%$ from analyses with different mesh refinement ($\gamma' = 20$ kN/m^3)

Fig. 7. Effect of K_0 on the load–settlement response for 2 m wide strip footings on Toyoura sand ($\gamma' = 20$ kN/m^3)

response for a 1 m footing on sand with $\gamma' = 20$ kN/m^3. This suggests that the pressure-level effect can be quantified effectively if the variation of N_γ is considered with respect to the product $\gamma'B$ instead of B alone. In fact, De Beer (1965) introduced the parameter $\gamma'B/E_q$ (where $E_q = p_a = 100$ kPa) to quantify the size effect. The validity of normalising with respect to $\gamma'B$ can be understood by considering the fact that the average p' in the collapse mechanism depends on the bearing pressure q_{bL} and the average geostatic (initial) stress, which both are linear functions of $\gamma'B$. Therefore, if two footings with dimensions B_1 and B_2 rest on uniform sand deposits with unit weights γ'_1 and γ'_2, and $\gamma'_1 B_1 = \gamma'_2 B_2$, they will exhibit the same average p' and, consequently, the same N_γ values. Fig. 12(a) shows N_γ resulting from FE analyses of strip footings with different sand relative densities. It can be seen that data points corresponding to the same $\gamma'B$ fall almost on top of each
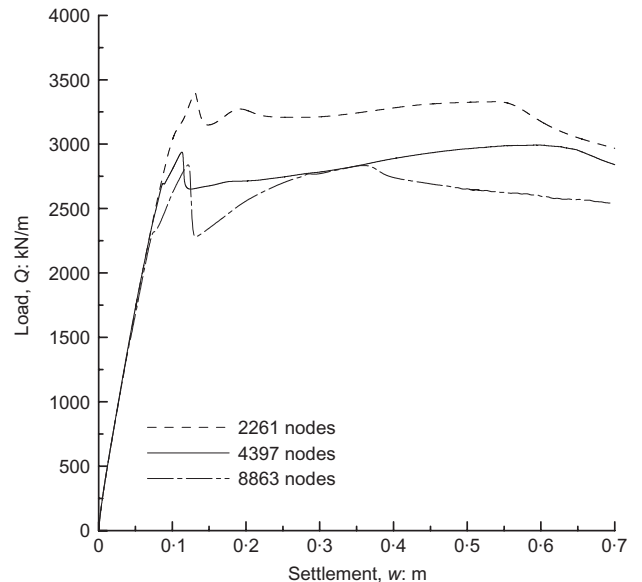
other. The same is also true for the equivalent bearing capacity factor $N_\gamma s_\gamma$ in the case of circular footings (Fig. 12(b)).

By dividing $N_\gamma s_\gamma$ by N_γ an s_γ value is obtained for circular footings that is derived on the basis of comparing footings resting on a given sand layer (same relative density), as opposed to an s_γ that is based on having the footings resting on materials with the same ϕ'. It is seen that s_γ turns out to be always less than unity, which is consistent with experimental data (De Beer, 1965; Ueno et al., 1998). This would initially appear to be in contrast with results from the MOC using the ABC program (Martin, 2003) or limit analysis (Michalowski, 2001; Lyamin et al., 2007). In reality, however, as discussed by Salgado (2008) and Lyamin et al. (2007), it is the basis of comparison of strip and circular footings that is different. MOC, limit analysis and FE analyses (Manoharan & Dasgupta, 1995; Loukidis & Salgado, 2009b), assuming that the soil follows the Mohr–Coulomb (M–C) failure criterion (same friction angle irrespective of nearly triaxial compression conditions or plane-strain conditions), will indeed produce $s_\gamma > 1$. But, in reality, the friction angle under triaxial compression conditions is smaller than that under plane-strain conditions for the same D_R, which leads to $s_\gamma < 1$ if D_R is the basis of comparison.

In Fig. 13, N_γ for strip footings and $N_\gamma s_\gamma$ for circular footings on Toyoura sand are plotted against the normalised footing width $\gamma'B/p_a$. The inclination of the curves becomes shallower as the sand relative density decreases. This suggests that the pressure effect becomes less important for loose sands than for dense sands. The results for strip footings on Toyoura sand (Fig. 13) can be closely approximated by the equation

$$N_\gamma = 2.82 \exp\left(3.64 \frac{D_R}{100\%}\right)\left(\frac{\gamma'B}{p_a}\right)^{-0.4} \quad (3)$$

Figure 14 shows the values of the shape factor s_γ derived from the FE analysis results. These values can be approximated by the equation

$$s_\gamma^{circ} = 1 - 0.23 \frac{D_R}{100\%} \quad (4)$$
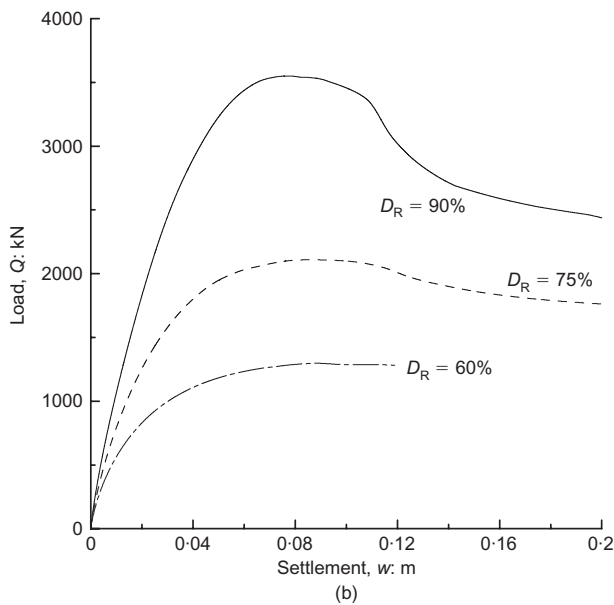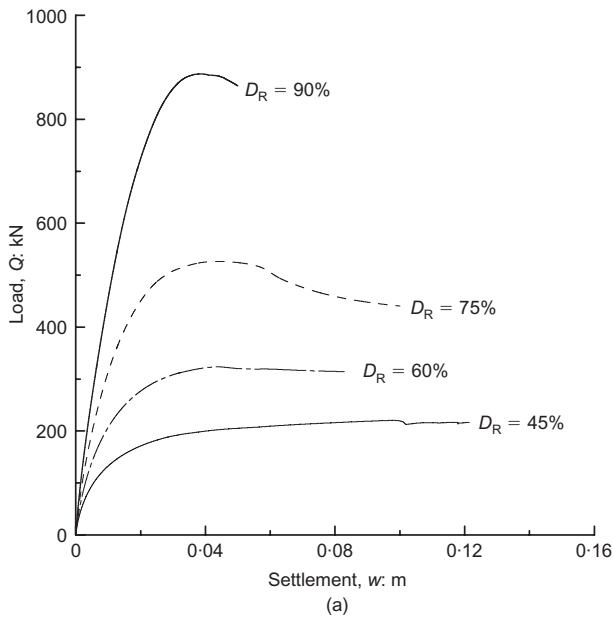
(a)

(b)

Fig. 9. Load–settlement response from analyses of circular footings on Toyoura sand: (a) diameter 1 m, effective unit weight 20 kN/m³; (b) diameter 2 m, effective unit weight 10 kN/m³
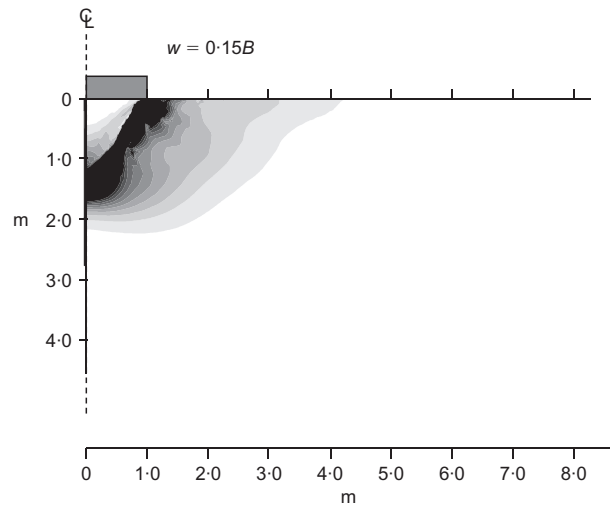

Fig. 10. Contours of incremental plastic maximum shear strain from analysis of circular footing on dense Toyoura sand ($B = 2$ m, $\gamma' = 10$ kN/m³, $D_R = 90\%$)
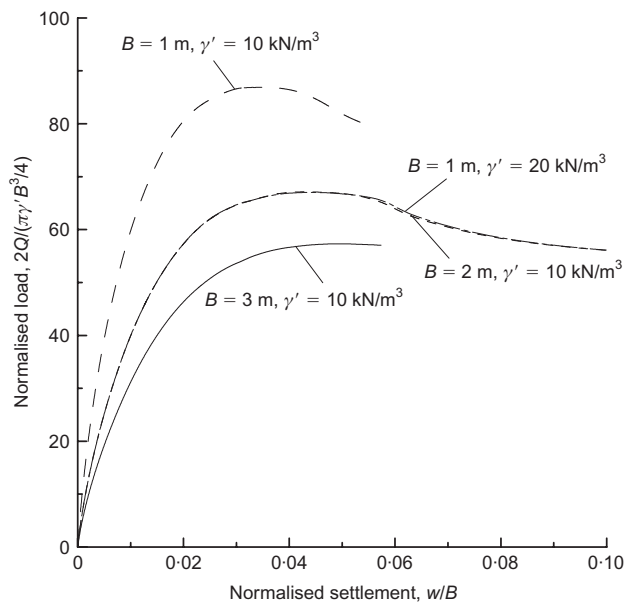

Fig. 11. Normalised load–normalised settlement curves from analyses of circular footings on Toyoura sand with $D_R = 75\%$ for different footing diameters and soil unit weight values

Data compiled by De Beer (1965) suggest that, for circular footings, the shape factor s_γ is approximately 0·6. The FE analysis results suggest that the shape factor is in the range 0·74–0·9, with the s_γ values decreasing with increasing relative density. The De Beer (1965) estimate is based on data from 1*g* model tests with small model footing widths ($\gamma' B/p_a$ of about 0·02) performed on one type of sand. However, a closer look at other data collected and cited by De Beer (1965) suggests that the shape factor value is between 0·7 and 0·9. In addition, centrifuge data for Toyoura sand suggest that $s_\gamma = 0·6$ constitutes a lower bound (Ueno *et al.*, 2001), with the actual shape factor values more likely to be in the range 0·70–0·82.

From Fig. 15 it can be concluded that, for the same footing size, soil unit weight and relative density, the limit load of a footing resting on medium dense to dense clean Ottawa sand is smaller than that of a footing resting on Toyoura sand, arguably because Ottawa sand, which has round to sub-round grains, has smaller shear strength than Toyoura sand, which has sub-angular to angular grains. This

fact is reflected directly in the difference between the critical-state friction angle values of the two sands.

The results from the present FE analyses are compared with experimental data in Fig. 16. The experimental data come from centrifuge tests using Toyoura sand with relative densities ranging from 58% to 88% reported by Tatsuoka *et al.* (1991) and Ueno *et al.* (1998). Comparison at the specific relative densities at which the tests were performed is achieved with the help of equations (3) and (4). The FE-based curves match the general trend. However, the curves generally plot lower than the corresponding experimental data, with average deviation around 20% and a maximum deviation of 50%. This discrepancy, which is expected, can be attributed to the following factors.

(*a*) The particle size effect, as discussed previously, renders the collapse loads resulting from centrifuge tests larger than those exhibited by the prototypes they are intended to simulate (Tatsuoka *et al.*, 1994, 1997; Siddiquee *et al.*, 1999; Tejchman & Herle, 1999). The magnitude of
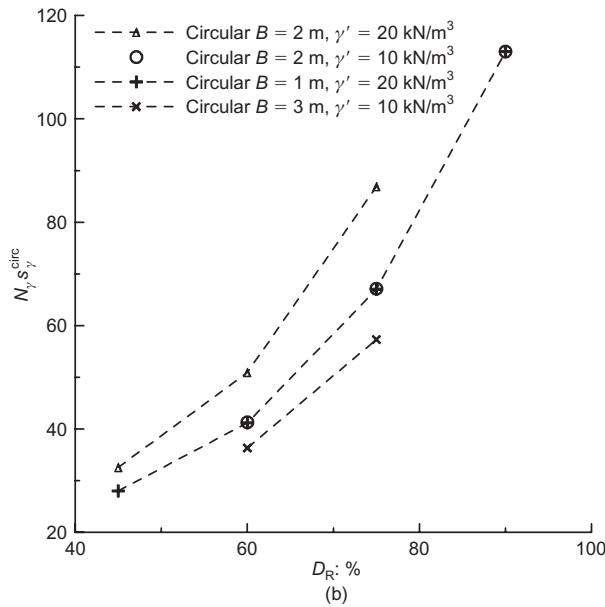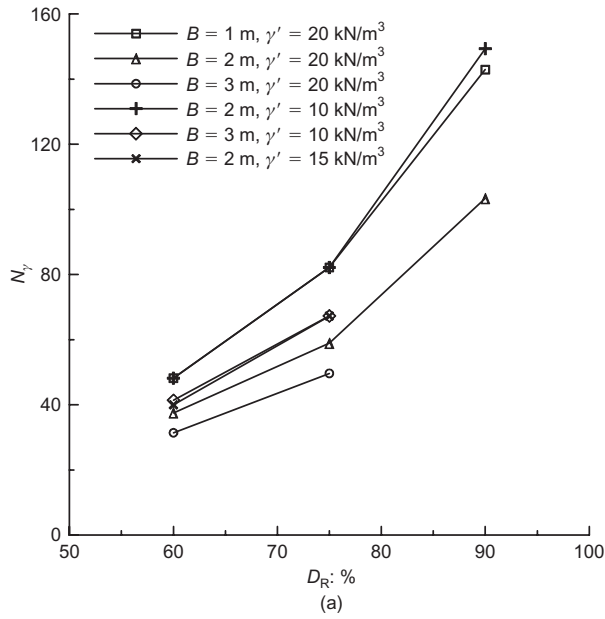
Fig. 12. (a) N_γ for strip footings and (b) $N_\gamma s_\gamma$ for circular footings resting on Toyoura sand with various relative densities
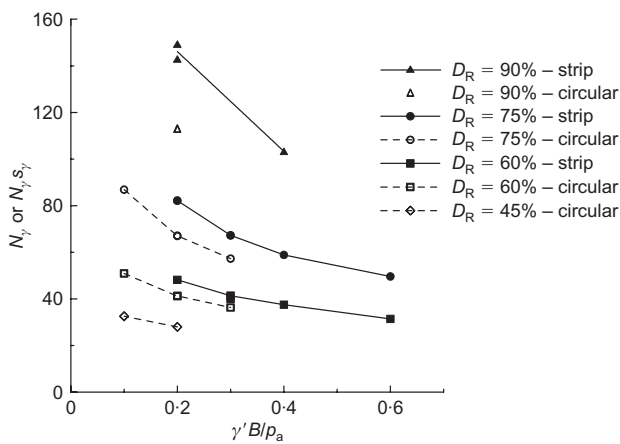

Fig. 13. Pressure-level effect on bearing capacity factor N_γ for strip footings and $N_\gamma s_\gamma$ for circular footings on Toyoura sand
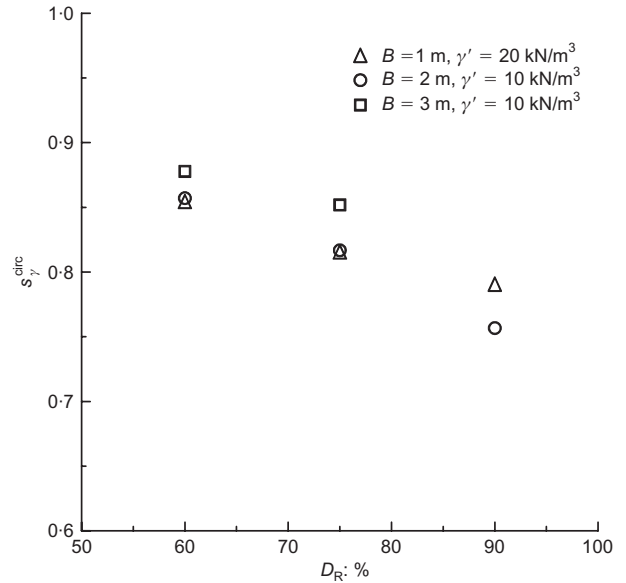

Fig. 14. Shape factor for circular footings based on results from FE analyses of footings on Toyoura sand

the deviations of the FE-based predictions of the response of the prototype footings from centrifuge data modelling the same footings is consistent with observations by Tatsuoka *et al.* (1991).

(b) The FE analyses follow a small-strain formulation, meaning that they neglect the generation of embedment (and consequently of surcharge) as the footing penetrates further into the sand (large-deformation effects become important for medium dense and loose sand). This effect of embedment build-up on the bearing capacity of surface footings was clearly demonstrated by Nova & Montrasio (1991), who performed tests on model footings on sand with and without removing the embedment build-up above the footing base level as the model footings penetrated in the soil.

Equivalent friction angle value

Given that the current state of practice consists of using the bearing capacity equation with factors based on the MOC, it is of interest to find what is the appropriate ϕ' value to be used in the bearing capacity equation (equation (1)). The N_γ resulting from the FE analyses can be used to back-calculate a friction angle using equation (2). This friction angle value can be considered an equivalent ('average') friction angle ϕ_{eq} that automatically takes into account the sand anisotropy and progressive failure.

Figure 17 show the difference between ϕ_{eq} values back-calculated using equation (2) and the corresponding critical state friction angle ϕ_c^{TXC} under triaxial compression conditions (unlike ϕ_c under PS conditions, ϕ_c^{TXC} can be estimated or measured with relative ease). Strip footings data for Toyoura sand and clean Ottawa sand have been grouped together. The subtraction of ϕ_c^{TXC} from the equivalent friction angle is done to account for the differences between the strength of different sands. It is evident that, for $\gamma'B/p_a$ in the range encountered in practice $(0\cdot1-0\cdot6)$ and for a given D_R, ϕ_{eq} values may vary by as much as 4°. The data shown in Fig. 17 can be fitted using the correlation

$$\phi_{eq} = \phi_c^{TXC} + \left\{ \left[17\cdot6\left(\frac{D_R}{100\%}\right) - 8\cdot8 \right] - 2\cdot44\ln\left(\frac{B\gamma'}{p_a}\right) \right\}$$
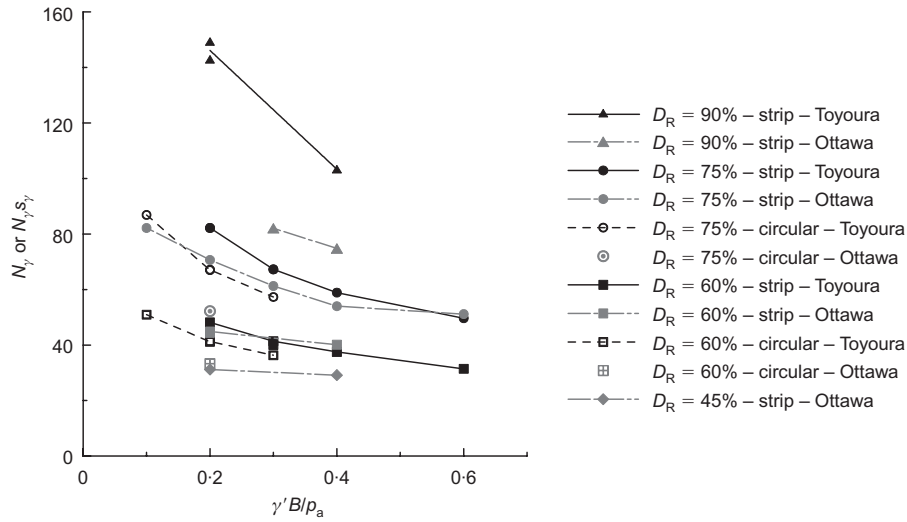
(5)

Fig. 15. Comparison between bearing capacity factors N_γ (strip footings) and $N_\gamma s_\gamma$ (circular footings) resulting from analyses with Toyoura sand and clean Ottawa sand

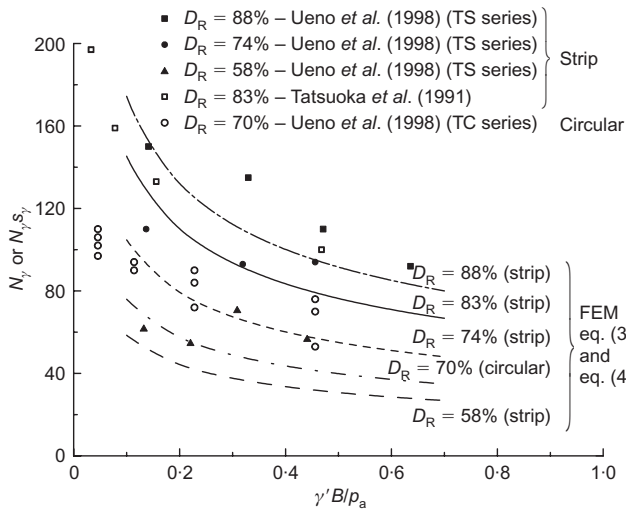**Fig. 16. Comparison between experimental data from centrifuge tests and predictions based on FE results using equations (3) and (4)**
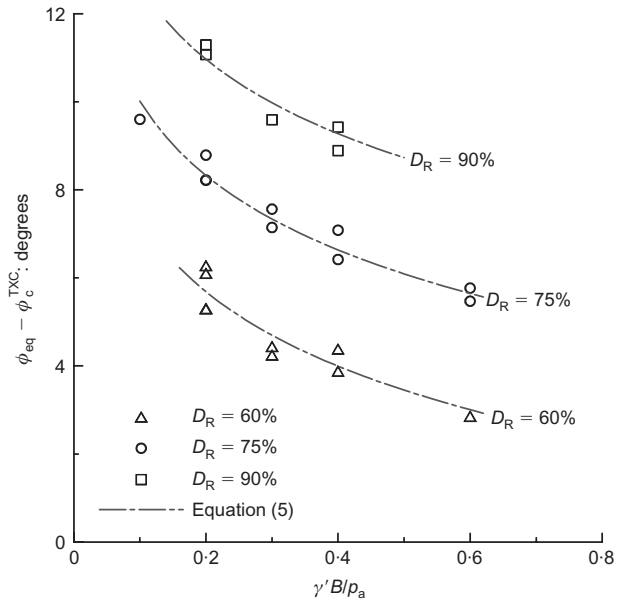

Fig. 17. Difference between equivalent friction angle and critical state friction angle in triaxial compression (TXC), as a function of relative density and normalised footing width

Using the equivalent friction angle from the above equation, estimates of the bearing capacity of strip footings can be made by calculating an N_γ value that takes directly into account the effects of pressure level, sand density and progressive failure. The bearing capacity of circular footings may be computed using the shape factor calculated using equation (4).

perfectly. The FE results suggest that the shape factor for circular footings, for a fixed relative density, is in the range 0·7–0·9. Finally, FE analysis results can be used to obtain useful correlations for N_γ, s_γ and an equivalent friction angle to be used in the classical bearing capacity equation.

CONCLUSIONS

A two-surface constitutive model was used in simulations of strip and circular footings resting on the surface of a uniform sand deposit. The FE simulations of strip footings show that full formation of the general shear mechanism occurs at large settlements. For dense sands these settlements can be significantly larger than those required for reaching the limit (collapse) load, which are in a wide range from 5% to 30% of the footing width B, depending on the relative density and sand intrinsic properties. The bearing capacity factor N_γ decreases with increasing footing width and sand unit weight. The normalisation parameter $\gamma'B/p_a$ proposed by De Beer (1965) quantifies the pressure level effect almost

NOTATION

B	footing width
b	intermediate principal stress ratio
D_R	relative density
D_{50}	mean particle size
E_q	stress normalising factor (100 kPa)

K_0	coefficient of earth pressure at rest
N_q	bearing capacity factor for surcharge
N_γ	bearing capacity factor for soil weight
p'	mean effective stress
p_a	atmospheric pressure
Q	load
Q_L	collapse (limit) load
q_{bL}	limit bearing pressure
s_γ	shape factor
w	settlement
w_L	settlement at limit load
γ'	soil effective unit weight
$\Delta\gamma^p_{max}$	incremental maximum plastic shear strain
$\sigma'_1, \sigma'_2, \sigma'_3$	principal effective stresses
ϕ'	effective friction angle
ϕ_c	critical state friction angle
ϕ_c^{TXC}	critical state friction angle under triaxial compression
ϕ_{eq}	equivalent friction angle
ψ_{dil}	dilatancy angle

REFERENCES

Abbo, A. J. & Sloan, S. W. (2000). *SNAC, User manual, Version 2·0*. Department of Civil, Surveying and Environmental Engineering, University of Newcastle, Callaghan, Australia.

Abelev, A. V. & Lade, P. V. (2004). Characterization of failure in cross-anisotropic soils. *J. Engng Mech. ASCE* **130**, No. 5, 599–606.

Aiban, S. A. & Znidarčić, D. (1995). Centrifugal modeling of bearing capacity of shallow foundations on sands. *J. Geotech. Engng ASCE* **121**, No. 10, 704–712.

Brinch Hansen, J. (1970). A revised and extended formula for bearing capacity. *Danish Geotech. Inst. Bull.* **28**, 5–11.

Carraro, J. A. H. (2004). *Mechanical behavior of silty and clayey sands*. PhD dissertation, Purdue University.

Carraro, J. A. H., Bandini, P. & Salgado, R. (2003). Liquefaction resistance of clean and nonplastic silty sands based on cone penetration resistance. *J. Geotech. Geoenviron. Engng ASCE* **129**, No. 11, 965–976.

Dafalias, Y. F. & Manzari, M. T. (2004). Simple plasticity sand model accounting for fabric change effects. *J. Engng Mech. ASCE* **130**, No. 6, 622–634.

Dafalias, Y. F., Papadimitriou, A. G. & Li, X. S. (2004). Sand plasticity model accounting for inherent fabric anisotropy. *J. Engng Mech. ASCE* **130**, No. 11, 1319–1333.

De Beer, E. E. (1965). Bearing capacity and settlement of shallow foundations on sand. *Proceedings of the symposium on bearing capacity and settlement of foundations*, Durham, NC, pp. 15–33.

Fukushima, S. & Tatsuoka, F. (1984). Strength and deformation characteristics of saturated sand at extremely low pressures. *Soils Found.* **24**, No. 4, 30–48.

Hardin, B. O. & Richart, F. E. Jr. (1963). Elastic wave velocities in granular soils. *J. Soil Mech. Found. Div. ASCE* **89**, No. SM1, 33–65.

Iwasaki, T., Tatsuoka, F. & Takagi, Y. (1978). Shear moduli of sands under cyclic torsional shear loading. *Soils Found.* **18**, No. 1, 39–56.

Kimura, T., Kusakabe, O. & Saitoh, K. (1985). Geotechnical model tests of bearing capacity problems in a centrifuge. *Géotechnique* **35**, No. 1, 33–45, doi: 10.1680/geot.1985.35.1.33.

Kutter, B. L., Abghari, A. & Cheney, J. A. (1988). Strength parameters for bearing capacity of sand. *J. Geotech. Engng* **114**, No. 4, 491–498.

Lam, W.-K. & Tatsuoka, F. (1988). Effects of initial anisotropic fabric and σ_2 on strength and deformation characteristics of sand. *Soils Found.* **28**, No. 1, 89–106.

Li, X. S. & Dafalias, Y. F. (2000). Dilatancy of cohesionless soils. *Géotechnique* **50**, No. 4, 449–460, doi: 10.1680/geot.2000.50.4.449.

Li, X. S., Dafalias, Y. F. & Wang, Z. L. (1999). State-dependent dilatancy in critical state constitutive modeling of sand. *Can. Geotech. J.* **36**, No. 4, 599–611.

Loukidis, D. (2006). *Advanced constitutive modeling of sands and applications to foundation engineering*. PhD dissertation, Purdue University.

Loukidis, D. & Salgado, R. (2008). Analysis of the shaft resistance of non-displacement piles in sand. *Géotechnique* **58**, No. 4, 283–296, doi: 10.1680/geot.2008.58.4.283.

Loukidis, D. & Salgado, R. (2009a). Modeling sand response using two-surface plasticity. *Comput. Geotech.* **36**, No. 1–2, 166–186.

Loukidis, D. & Salgado, R. (2009b). Bearing capacity of strip and circular footings in sand using finite elements. *Comput. Geotech.* **36**, No. 6, 871–879.

Lyamin, A., Salgado, R., Sloan, S. W. & Prezzi, M. (2007). Two- and three-dimensional bearing capacity of footings in sand. *Géotechnique* **57**, No. 8, 647–662, doi: 10.1680/geot.2007.57.8.647.

Manoharan, N. & Dasgupta, S. P. (1995). Bearing capacity of surface footings by finite elements. *Comput. Struct.* **54**, No. 4, 563–586.

Manzari, M. T. & Dafalias, Y. F. (1997). A critical state two-surface plasticity model for sands. *Géotechnique* **47**, No. 2, 255–272, doi: 10.1680/geot.1997.47.2.255.

Martin, C. M. (2003). *User guide for ABC – Analysis of Bearing Capacity, Version 1·0*. Department of Engineering Science, University of Oxford, OUEL Report No. 2261/03.

Martin, C. M. (2005). Exact bearing capacity calculations using the method of characteristics. *Proc. 11th Int. Conf. of the International Association for Computer Methods and Advances in Geomechanics, Turin* **4**, 441–450.

Meyerhof, G. G. (1963). Some recent research on the bearing capacity of foundations. *Can. Geotech. J.* **1**, No. 1, 16–26.

Michalowski, R. L. (2001). Upper-bound load estimates on square and rectangular footings. *Géotechnique* **51**, No. 9, 787–798.

Murthy, T. G. (2006). *Study of the undrained static response of sandy soils in the critical state framework*. PhD dissertation, Purdue University.

Murthy, T. G., Loukidis, D., Carraro, J. A. H, Prezzi, M. & Salgado, R. (2007). Undrained monotonic response of clean and silty sands. *Géotechnique* **57**, No. 3, 273–288, doi: 10.1680/geot.2007.57.3.273.

Nakata, Y., Hyodo, M., Murata, H. & Yasufuku, N. (1998). Flow deformation of sands subjected to principal stress rotation. *Soils Found.* **38**, No. 2, 115–128.

Nova, R. & Montrasio, L. (1991). Settlements of shallow foundations on sand. *Géotechnique* **41**, No. 2, 243–256, doi: 10.1680/geot.1991.41.2.243.

Oda, M. (1972). Initial fabrics and their relations to mechanical properties of granular material. *Soils Found.* **12**, No. 1, 17–36.

Papadimitriou, A. G. & Bouckovalas, G. D. (2002). Plasticity model for sand under small and large cyclic strains: a multiaxial formulation. *Soil Dynam. Earthquake Engng* **22**, No. 3, 191–204.

Perkins, S. W. & Madson, C. R. (2000). Bearing capacity of shallow foundations on sand: a relative density approach. *J. Geotech. Geoenviron. Engng ASCE* **126**, No. 6, 521–530.

Salgado, R. (2008). *The engineering of foundations*. New York: McGraw-Hill.

Siddiquee, M. S. A., Tanaka, T., Tatsuoka, F., Tani, K. & Morimoto, T. (1999). Numerical simulation of bearing capacity characteristics of strip footing on sand. *Soils Found.* **39**, No. 4, 93–109.

Sloan, S. W. & Randolph, M. F. (1982). Numerical prediction of collapse loads using finite element methods. *Int. J. Numer. Anal. Methods Geomech.* **6**, No. 1, 47–76.

Tatsuoka, F., Sakamoto, M., Kawamura, T. & Fukushima, S. (1986). Strength and deformation characteristics of sand in plane strain compression at extremely low pressures. *Soils Found.* **26**, No. 1, 65–84.

Tatsuoka, F., Okahara, M., Tanaka, T., Tani, K., Morimoto, T. & Siddiquee, M. S. A. (1991). Progressive failure and particle size effect in bearing capacity of a footing on sand. *Proceedings of the Geotechnical Engineering Congress*, GSP 27, pp. 788–802. Reston, VA: ASCE.

Tatsuoka, F., Siddiquee, M. S. A. & Tanaka, T. (1994). Link among design, model tests, theories and sand properties in bearing capacity of footing on sand. *Proc. 13th Int. Conf. Soil Mech. Found. Engng, New Delhi* **5**, 87–88.

Tatsuoka, F., Goto, S., Tanaka, T., Tani, K. & Kimura, Y. (1997). Particle size effects on bearing capacity of footing on granular material. In *Deformation and progressive failure in geomechanics* (eds A. Asaoka, T. Adachi and F. Oka), pp. 133–138. Oxford: Pergamon.

Tejchman, J. & Herle, I. (1999). A 'class A' prediction of the bearing capacity of plane strain footings on sand. *Soils Found.* **39**, No. 5, 47–60.

Ueno, K., Miura, K. & Maeda, Y. (1998). Prediction of ultimate bearing capacity of surface footings with regard to size effects. *Soils Found.* **38**, No. 3, 165–178.

Ueno, K., Miura, K., Kusakabe, O. & Nishimura, M. (2001). Reappraisal of size effect of bearing capacity from plastic solution. *J. Geotech. Geoenviron. Engng ASCE* **127**, No. 3, 275–281.

Vesić, A. S. (1973). Analysis of ultimate loads of shallow foundations. *J. Soil Mech. Found. Div. ASCE* **99**, No. 1, 45–73.

Yoshimine, M., Ishihara, K. & Vargas, W. (1998). Effects of principal stress direction and intermediate principal stress on undrained shear behavior of sand. *Soils Found.* **38**, No. 3, 179–188.